

Majorana Crystal in Rhombohedral Graphene

Chiho Yoon and Fan Zhang

Department of Physics, University of Texas at Dallas, Richardson, Texas 75080, USA

(Dated: March 18, 2026)

Recent experiments in rhombohedral graphene report an unusual superconducting phase emerging from a spin- and valley-polarized quarter-metal state. The prevailing interpretation invokes chiral topological superconductivity, but the role of the ‘Fulde-Ferrell’ phase factor due to intra-valley pairing has remained largely unexplored. Here we show, via a gauge transformation, that this phase is equivalent to an ordinary chiral topological superconductor on the triangular lattice, while simultaneously forming an extraordinary Majorana crystal on the dual honeycomb lattice reminiscent of the Haldane model.

Introduction—Superconductivity, magnetism, topology, and fractionalization lie at the heart of condensed matter physics. Few-layer graphene with rhombohedral stacking has long been theoretically recognized as fertile ground for correlated and topological physics and is now experimentally realized as a highly tunable platform for exploring these phenomena and beyond [1–25]. This family of 2D semiconductors provides a rare opportunity to study the coexistence and interplay of all four fundamental themes within a single material. Recently, an unprecedented superconducting phase was observed emerging from a spin- and valley-polarized quarter-metal state, offering a unique setting to unify these themes. While theoretical studies consistently identify this phase as a chiral topological superconductor, the effects of the finite momentum carried by Cooper pairs due to intra-valley pairing have so far been neglected, despite their potential significance [26–35].

Pair-density-wave (PDW) superconductivity, characterized by Cooper pairing at finite center-of-mass momentum, is a recurring phase in unconventional superconductors [36–40]. Originally proposed by Fulde and Ferrell (FF) [41] and Larkin and Ovchinnikov (LO) [42] in the context of magnetic-field-induced instabilities, the concept has since broadened beyond its original setting. FF-type PDWs, where the Cooper-pair momentum takes a single finite value, have received comparatively little attention. They are stabilized only under restrictive conditions that explicitly break both time-reversal and inversion symmetries, e.g., strong Zeeman fields or spin-orbit couplings, limiting experimental feasibility. Unlike other PDWs, FF states lack spatial amplitude modulation and thus few readily observable signatures. Moreover, an FF state can be locally gauge-transformed into a zero-momentum superconductor, making it often only weakly distinguishable from uniform superconductivity.

However, the intra-valley chiral PDW state is qualitatively distinct. First, it requires neither a Zeeman field nor spin-orbit coupling, as the breaking of time-reversal and inversion symmetries is intrinsic to the quarter-metal state. Second, the spatial modulation resides in the pairing phase rather than the amplitude. Third, unlike conventional cases, the Fermi surface is extremely small whereas the Cooper-pair momentum is extremely large. Fourth, the Cooper-pair momentum $2K$ (or $2K'$) is a special vector invariant under C_{3z} . Taken together, these features suggest that this PDW is inherently 2D. In par-

ticular, the seemingly FF-like phase factor $e^{i2K \cdot \mathbf{R}}$ may instead be interpreted as a symmetric superposition $\sum_{j=1,2,3} e^{i2K_j \cdot \mathbf{R}}$, where K_j ($j=1,2,3$) are the three vectors generated by C_{3z} acting on K . This naturally raises the question of what are the physical implications of such a pairing structure, and how the intra-valley chiral PDW differs from both a conventional FF state and a zero-momentum spinless chiral superconductor.

Here we demonstrate that the intra- K -valley chiral PDW state is equivalent to a zero-momentum topological chiral p -wave superconductor on the triangular sublattice to which the electrons are polarized, with an emergent low-energy Majorana crystal localized on the dual honeycomb sublattice. The Peierls phase associated with the momentum shift between the Γ and K points, corresponding to a $\pm\pi$ flux per triangle, is naturally and exactly generated by the vortex-antivortex lattice that hosts the Majorana crystal. The resulting Majorana crystal model, reminiscent of the Haldane model, has a direct or indirect energy gap and carries a nontrivial Chern number of ± 1 .

Topological superconductor—We begin with a description of a chiral p -wave topological superconductor on the triangular lattice, which we will refer to as the A sublattice. The corresponding Bogoliubov-de Gennes (BdG) Hamiltonian consists of the chemical potential term, the normal state Hamiltonian \hat{H}_N , and the superconducting order parameter term \hat{H}_Δ :

$$\begin{aligned} \hat{H}_N &= \sum_{\mathbf{R}} \sum_{l=1,2,3} t_{\mathbf{R}+\mathbf{a}_l, \mathbf{R}} e^{\frac{ie}{\hbar c} \int_{\mathbf{R}}^{\mathbf{R}+\mathbf{a}_l} \mathbf{A} \cdot d\mathbf{l}} c_{\mathbf{R}+\mathbf{a}_l}^\dagger c_{\mathbf{R}} + \text{H.c.}, \\ \hat{H}_\Delta &= \sum_{\mathbf{R}} \sum_{l=1,2,3} \Delta_{\mathbf{R}+\mathbf{a}_l, \mathbf{R}} \omega^l c_{\mathbf{R}+\mathbf{a}_l}^\dagger c_{\mathbf{R}}^\dagger + \text{H.c.}, \end{aligned} \quad (1)$$

where $c_{\mathbf{R}}^\dagger$ is the creation operator of an electron on the triangular A sublattice $\mathbf{R} = n_1 \mathbf{a}_1 + n_2 \mathbf{a}_2$ with the primitive lattice vectors $\mathbf{a}_1 = a(1, 0)$, $\mathbf{a}_2 = a(-1/2, \sqrt{3}/2)$, and $\mathbf{a}_3 = -\mathbf{a}_1 - \mathbf{a}_2$. $t_{\mathbf{R}+\mathbf{a}_l, \mathbf{R}} = -te^{i\alpha}$ ($t > 0$) is the nearest-neighbor hopping, which is isotropic and uniform because of the C_{3z} and translational symmetries. The Peierls phase encodes the magnetic flux associated with the gauge field \mathbf{A} . While $\omega = e^{2\pi i/3}$ encodes the phase winding of the chiral p -wave order parameter, $\Delta_{\mathbf{R}+\mathbf{a}_l, \mathbf{R}}$ denotes the center-of-mass superconducting phase, given by

$$\Delta_{\mathbf{R}+\mathbf{a}_l, \mathbf{R}} = \Delta_0 e^{i\theta(\mathbf{R})} \exp \left[\frac{i}{2} \int_{\mathbf{R}}^{\mathbf{R}+\mathbf{a}_l} \nabla \theta \cdot d\mathbf{l} \right], \quad (2)$$

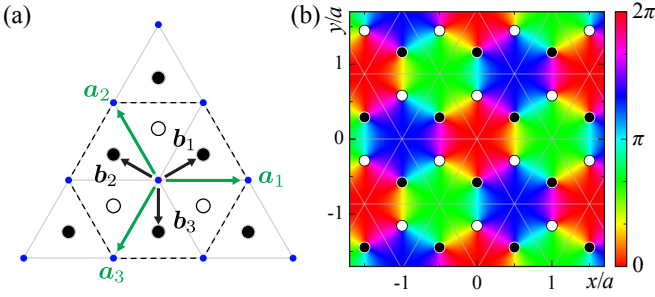


FIG. 1. (a) Embedded vortices (black dots) and antivortices (open dots) at the centers of the up and down triangles of a triangular lattice (blue dots). \mathbf{a}_1 and \mathbf{a}_2 are the primitive lattice vectors. $+\mathbf{b}_i$ and $-\mathbf{b}_i$ ($i = 1, 2, 3$) are the positions of vortices and antivortices relative to a lattice point, respectively. The blue dashed lines outline a $\sqrt{3} \times \sqrt{3}$ supercell. (b) Color plot of the superconducting phase field $\theta(\mathbf{r})$.

with $\Delta_0 > 0$. This equation provides a lattice regularization of the superconducting phase field $\theta(\mathbf{r})$ [43–45]. In the absence of magnetic field and (anti)vortex, $\mathbf{A} = 0$ and $\theta = 0$. In particular, the Cooper pair momentum is zero.

Now embed a vortex-antivortex lattice of vorticity $\pm N$ to the superconductor as follows:

$$\nabla \times \nabla \theta(\mathbf{r}) = 2\pi N \hat{z} \sum_{\mathbf{R}} \sum_{\tau=\pm} \tau \delta(\mathbf{r} - \mathbf{R} - \tau \mathbf{b}_1), \quad (3)$$

where $\mathbf{b}_1 = (2\mathbf{a}_1 + \mathbf{a}_2)/3$, $\mathbf{b}_2 = (2\mathbf{a}_2 + \mathbf{a}_3)/3$, and $\mathbf{b}_3 = -\mathbf{b}_1 - \mathbf{b}_2$. The vortices and antivortices are placed at the centers of the up and down triangles [Fig. 1(a)], respectively, which we hereafter denote as the C and B sublattices. This configuration corresponds to N flux quanta (one flux quantum: $\phi_0 = hc/2e$ or π magnetic flux) per triangle [46], equivalent to an effective field of 7.9×10^4 T for the lattice of graphene, with the flux sign alternating between the up and down triangles.

The natural solution of the superconducting phase field reads

$$\theta(\mathbf{r}) = N \sum_{\mathbf{R}} \sum_{\tau=\pm} \tau \arg(\mathbf{r} - \mathbf{R} - \tau \mathbf{b}_1) \text{ mod } 2\pi. \quad (4)$$

However, Eq. (4) is only conditionally convergent, because although the monopole moment of each unit cell vanishes, higher-order moments such as dipole and quadrupole may remain. This situation is analogous to the convergence issues encountered in the Ewald summation of ionic crystals [47]. To guarantee a well-defined $\theta(\mathbf{r})$, we construct the following minimal supercell [Fig. 1(a)] in which the monopole, dipole, and quadrupole moments all vanish, ensuring convergence:

$$\theta(\mathbf{r}) = N \sum_{\mathbf{R}'} \sum_{l=1,2,3} \sum_{\tau=\pm} \tau \arg(\mathbf{r} - \mathbf{R}' - \tau \mathbf{b}_l) \text{ mod } 2\pi, \quad (5)$$

where $\mathbf{R}' = n_1(2\mathbf{a}_1 + \mathbf{a}_2) + n_2(2\mathbf{a}_2 + \mathbf{a}_3)$ are the superlattice vectors. For a closed triangular path encircling a single (anti)vortex, one finds $\oint_{\Delta(\nabla)} \nabla \theta \cdot d\mathbf{l} = \pm 2N\pi$.

The C_{3z} symmetry further dictates $\int_{\mathbf{R}}^{\mathbf{R}+\mathbf{a}_l} \nabla \theta \cdot d\mathbf{l} = 2e/\hbar c \int_{\mathbf{R}}^{\mathbf{R}+\mathbf{a}_l} \mathbf{A} \cdot d\mathbf{l} = 2N\pi/3$ [48]. Therefore, in the presence of the vortex-antivortex lattice, the Peierls phase in Eq. (1)

is $N\pi/3$, and the order parameter in Eq. (2) is $\Delta_{\mathbf{R}+\mathbf{a}_l, \mathbf{R}} = \Delta_0 e^{i\theta(\mathbf{R})+iN\pi/3}$.

Gauge transformation—Under translations by the primitive lattice vectors \mathbf{a}_i , $\theta(\mathbf{r})$ is not invariant [Fig. 1(b)], whereas $\nabla \theta(\mathbf{r})$ is invariant, implying that $\theta(\mathbf{r} + \mathbf{a}_i) - \theta(\mathbf{r}) = \theta(\mathbf{R} + \mathbf{a}_i) - \theta(\mathbf{R}) = 2N\pi/3 \text{ mod } 2\pi$. It thus follows that under a lattice translation,

$$\theta(\mathbf{r} + \mathbf{R}) - \theta(\mathbf{r}) = 2N\mathbf{K} \cdot \mathbf{R} \text{ mod } 2\pi, \quad (6)$$

where $\mathbf{K} = (2\mathbf{G}_1 - \mathbf{G}_2)/3$. This superperiodicity implies that the shifted phase field $\tilde{\theta}(\mathbf{r}) = \theta(\mathbf{r}) - 2N\mathbf{K} \cdot \mathbf{r}$ has a restored lattice translational symmetry: $\tilde{\theta}(\mathbf{r}) = \tilde{\theta}(\mathbf{r} + \mathbf{R})$. This further implies $\tilde{\theta}(\mathbf{R}) = \tilde{\theta}(0) = \theta_0$, which can be chosen to be zero. Nevertheless, the order parameter reads

$$\Delta_{\mathbf{R}+\mathbf{a}_l, \mathbf{R}} = \Delta_0 e^{i(2N\mathbf{K}) \cdot (\mathbf{R} + \frac{\mathbf{a}_l}{2})} e^{i(N\pi + \theta_0)}. \quad (7)$$

Under the gauge transformation with $\chi(\mathbf{R}) = N\pi + \theta_0$, i.e.,

$$c_{\mathbf{R}}^{\dagger} \rightarrow e^{i\frac{1}{2}\chi(\mathbf{R})} c_{\mathbf{R}}^{\dagger}, \quad \mathbf{A} \rightarrow \mathbf{A} - \frac{\hbar c}{2e} \nabla \chi(\mathbf{R}),$$

$$\Delta_{\mathbf{R}+\mathbf{a}_l, \mathbf{R}} \rightarrow e^{-i\frac{1}{2}[\chi(\mathbf{R}) + \chi(\mathbf{R}+\mathbf{a}_l)]} \Delta_{\mathbf{R}+\mathbf{a}_l, \mathbf{R}}, \quad (8)$$

the Hamiltonians in Eq. (1) become

$$\hat{H}_N = \sum_{\mathbf{R}} \sum_{l=1,2,3} t e^{i(\alpha + \frac{N\pi}{3})} c_{\mathbf{R}+\mathbf{a}_l}^{\dagger} c_{\mathbf{R}} + \text{H.c.},$$

$$\hat{H}_{\Delta} = \sum_{\mathbf{R}} \sum_{l=1,2,3} \Delta_0 e^{i(2N\mathbf{K}) \cdot (\mathbf{R} + \frac{\mathbf{a}_l}{2})} \omega^l c_{\mathbf{R}+\mathbf{a}_l}^{\dagger} c_{\mathbf{R}} + \text{H.c.} \quad (9)$$

When $N = 3n$ ($n \in \mathbb{Z}$), the first phase factor in \hat{H}_{Δ} reduces to 1, amounting to the zero-momentum chiral p -wave pairing. When $N = 3n \pm 1$ ($n \in \mathbb{Z}$), $2N\mathbf{K}$ becomes $2\mathbf{K}$ ($2\mathbf{K}'$), and \hat{H}_{Δ} can describe a chiral p -wave PDW state as a result of intra-valley pairing within the valley K (K'). Note that the well-defined vorticity is $N \text{ mod } 3$ because of the C_{3z} symmetry.

The normal-state Hamiltonian \hat{H}_N acquires a Peierls phase of $N\pi/3$ for the electron hopping from \mathbf{R} to $\mathbf{R} + \mathbf{a}_l$. Hereafter, we focus on the $N = 1$ case for simplicity. The band energy reads $E(\mathbf{k}, \alpha) = -2t \sum_l \cos(\mathbf{k} \cdot \mathbf{a}_l + \alpha)$ and $E(\mathbf{k}, \alpha + \pi/3)$ without and with the vortex-antivortex lattice. Independent of the value of α , the global band minima of $E(\mathbf{k}, \alpha)$ can only occur at Γ , K , and/or K' points (see End Matter). For $0 < \alpha < \pi/3$, the band edge is at Γ point originally, whereas it shifts to K point because of the $\pi/3$ Peierls phase produced by the vortex-antivortex lattice (see End Matter).

Altogether, we have demonstrated that the spinless, K -valley-polarized, low-density, chiral p -wave superconductor on the triangular lattice is equivalent to a conventional Γ -valley chiral p -wave superconductor on the same lattice with an embedded vortex-antivortex lattice of vorticities ± 1 on the dual honeycomb lattice.

Majorana crystal—Because each (anti)vortex binds an unpaired Majorana bound state (MBSs) in the spinless Γ -valley chiral p -wave superconductor, the low-energy quasiparticles of the K -valley PDW state form a Majorana crystal on the B

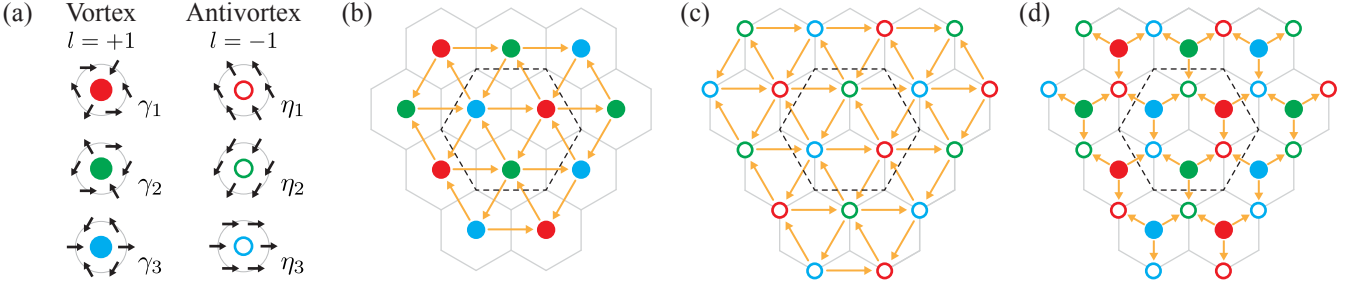


FIG. 2. (a) Schematics of the spatial phase-structures of the six types of MBSs, localized at vortex (solid circle) and antivortex (open circle) cores. Red, green, and blue colors indicate their phases of $2\pi/3$, $4\pi/3$, and 0 along the $+\hat{x}$ direction, respectively. Arrows indicate the corresponding phases. (b-d) Schematics of the the Majorana crystal relative to the graphene honeycomb lattice of the layer to which the electrons are polarized, as well as the (b) vortex-vortex, (c) antivortex-antivortex, and (d) vortex-antivortex couplings. The dashed lines outline the same $\sqrt{3} \times \sqrt{3}$ supercell shown in Fig 1(a).

and C triangular sublattices. Now, we construct a minimal two-band model consistent with C_{3z} symmetry and show that the Majorana bands carry a Chern number ± 1 .

We first characterize the MBSs created by γ_S^n and η_S^n at the cores of vortices and antivortices, respectively, in a spinless chiral $p_x + ip_y$ superconductor. The core positions are labeled by S and the vorticities by $\ell = \pm 1$. The MBSs take the form of

$$\frac{1}{\sqrt{2}} \left\{ e^{\frac{i}{2}[\phi_n + (\ell+1)\theta]} c_S + e^{-\frac{i}{2}[\phi_n + (\ell+1)\theta]} c_S^\dagger \right\} \quad (10)$$

in the continuum limit. Here c_S is a coherent superposition of all electron annihilation operators, the extra unit of winding beyond ℓ reflects the angular momentum of a uniform $p_x + ip_y$ pairing field, and ϕ_n denotes the phase along the $+\hat{x}$ direction. In general, the relative phase intrinsic to a MBS enclosing a vortex core winds twice faster than θ , whereas it remains a constant when enclosing an antivortex core.

For the MBSs on the honeycomb lattice, the continuous rotational symmetry reduces to C_{3z} symmetry. Thus, $\phi_n = 2\pi n/3$ can be chosen, to ensure their $\pm 2\pi/3$ differences dictated by C_{3z} symmetry. Figure 2(a) sketches the spatial phase-structures of the six types of MBSs. Under the C_{3z} rotation around the (anti)vortex core S , $C_{3z} \gamma_S^n C_{3z}^{-1} = \gamma_S^{n+1}$ and $C_{3z} \eta_S^n C_{3z}^{-1} = \eta_S^n$. However, the C_{3z} center can be any lattice site of the A, B, or C sublattice, and the $p_x + ip_y$ PDW state as a result of intra- K -valley pairing respects the C_{3z}^A , C_{3z}^B , and C_{3z}^C symmetries following the \bar{E}_K irreducible representation [32]. In short, while \hat{H}_N is invariant under the C_{3z}^A , C_{3z}^B , and C_{3z}^C operations, \hat{H}_Δ acquires a phase factor $\bar{\omega}$, 1 , and ω , respectively.

This implies that, besides the rotational symmetry C_{3z}^B , both \hat{H}_N and \hat{H}_Δ are invariant under the *projective* rotational symmetries $\tilde{C}_{3z}^A = C_{3z}^A \omega^{\tau_z}$ and $\tilde{C}_{3z}^C = C_{3z}^C \bar{\omega}^{\tau_z}$ for the BdG Hamiltonian, where τ_z acts on the Nambu particle-hole space. Correspondingly, as summarized in Table I, the transformations of γ_S^n and η_S^n under the projective symmetry operations are modified from those under the normal rotations. We note that the MBS configuration shown in Fig. 2 is consistent with these symmetry considerations, as well as the superperiodicity spec-

ified in Eq. (6). Remarkably, this configuration is in fact the only possibility to embed a single vortex-antivortex pair per original unit cell that is compatible with the \bar{E}_K irreducible representation: a vortex at the C sublattice site and an antivortex at the B sublattice site.

We then consider the couplings between MBSs. For simplicity, we include only three types of nearest-neighbor couplings, i.e., vortex-vortex (vv), antivortex-antivortex (aa), and vortex-antivortex (va), which are depicted in Figs. 2(c-e). It is straightforward to show that by imposing the \tilde{C}_{3z}^A , C_{3z}^B , \tilde{C}_{3z}^C , and translational symmetries, all the coupling amplitudes are identical within the same type. We denote the three types of couplings by t_{vv} , t_{aa} , and $t_{va} \in \mathbb{R}$, respectively. This isotropy and uniformity are consistent with the rule of Josephson coupling between two (anti)vortices [49].

Thus, the low-energy Majorana crystal (MC) model reads

$$\hat{H}_{MC} = \sum_{\langle ij \rangle} it_{va} \gamma_i \eta_j + \sum_{\langle\langle ij \rangle\rangle} (it_{vv} \gamma_i \gamma_j + it_{aa} \eta_i \eta_j), \quad (11)$$

where $\langle ij \rangle$ and $\langle\langle ij \rangle\rangle$ denote the nearest-neighbor and next-nearest-neighbor pairs on the honeycomb lattice formed by the MBSs. The order of the two Majorana operators in Eq. (11) follows the tail-to-head convention in Fig. 2.

The structure of Eq. (11) mirrors that of the Haldane model [50] with purely imaginary hoppings and vanishing staggered potential. Figure 3(a) shows the phase diagram of this Haldane model of Majoranas. Specifically, t_{va} couples the two different sublattices, producing the Majorana-band Dirac cones at the K and K' points shown in Fig. 3(b). Furthermore,

TABLE I. Transformation rules of the Majorana operators under the three (projective) C_{3z} rotations, e.g., $\tilde{C}_{3z}^A \gamma_S^n (\tilde{C}_{3z}^A)^{-1} = \gamma_{C_{3z}^A S}^{n-1}$.

Operator	\tilde{C}_{3z}^A	C_{3z}^B	\tilde{C}_{3z}^C
γ_S^n	$\gamma_{C_{3z}^A S}^{n-1}$	$\gamma_{C_{3z}^B S}^{n+1}$	$\gamma_{C_{3z}^C S}^n$
η_S^n	$\eta_{C_{3z}^A S}^{n+1}$	$\eta_{C_{3z}^B S}^n$	$\eta_{C_{3z}^C S}^{n-1}$

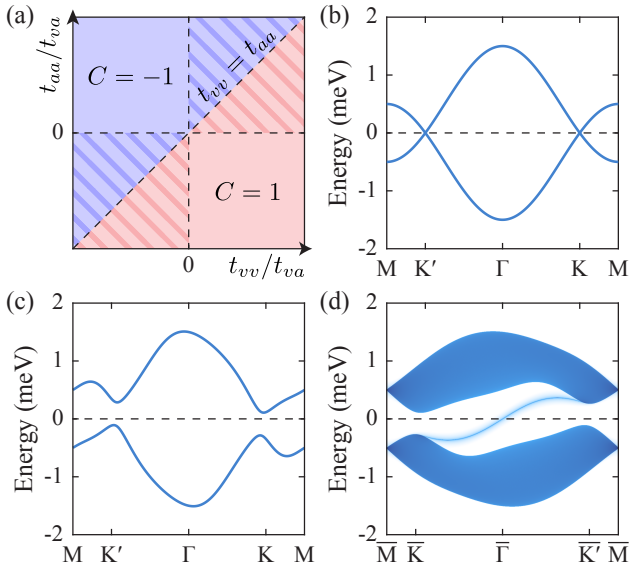


FIG. 3. (a) The phase diagram of the Majorana crystal model Eq. (11). The Chern number is 1 (−1) for the light red (blue) region. There is no indirect gap in the shaded region. (b) The Majorana-band Dirac cones at the K and K' points for the case with $t_{vv} = t_{aa} = 0$ and $t_{va} = 1$ meV. (c) The bulk and (d) the armchair-edge Majorana band structures for the case with $t_{vv} = 1/5$, $t_{aa} = -1/15$, and $t_{va} = 1$ meV.

$t_v - t_a$ gives rise to the Haldane gap, while $t_v + t_a$ provides opposite energy shifts in the two valleys respecting the particle-hole symmetry, as exemplified in Fig. 3(c).

The Majorana crystal model Eq. (11) reflects the direct vs. indirect gap nature and the topological character of the intra- K -valley chiral PDW state. The two Majorana bands are directly gapped as long as $t_{vv} \neq t_{aa}$ and $t_{va} \neq 0$, and the global gap exists when $t_{vv}t_{aa} < 0$. The Chern number is determined by $C = \text{sgn}(t_{vv} - t_{aa})$. Figure 3(d) presents the spectrum of the Majorana crystal with an armchair edge in a fully gapped case, obtained using the surface Green's function method. Evidently, a single chiral Majorana edge state emerges.

Discussion—In rhombohedral graphene, the large-electric-field-gapped bands are ultra-flat at low electron densities. The valley-polarized quarter-metal bands are mainly determined by the emergent order parameter, which acts as a Haldane mass at low energy, producing opposite energy shifts in the two valleys. Moreover, the low-energy electrons are polarized onto a single triangular sublattice of the outermost layer. Consequently, this order parameter can be modeled by $E(\mathbf{k}, \pi/2)$, implying that the quarter-metal superconductivity is equivalent to a Γ -valley chiral p -wave superconductor on the same sublattice, described by $\alpha = \pi/6$ in Eq. (1), while simultaneously forming a Majorana crystal on the other two sublattices.

We have assumed a vanishing penetration depth, $\lambda_L = 0$, for simplicity, although this assumption can be relaxed. For finite λ_L , the relation $\mathbf{A} = (\Phi_0/2\pi)\nabla\theta$ no longer holds, and the fluxoid quantization, including the contribution from the

loop current, reads

$$\oint \mathbf{A} \cdot d\mathbf{l} = \frac{\Phi_0}{2\pi} \oint \nabla\theta \cdot d\mathbf{l} - \frac{4\pi\lambda_L^2}{c} \oint \mathbf{j}_s \cdot d\mathbf{l}. \quad (12)$$

Consequently, the loop current modifies the π magnetic flux per triangle, or equivalently, the $\pi/3$ Peierls phase induced by the embedded vortex-antivortex lattice.

From the phase perspective, we have identified six types of MBSs allowed by the symmetries. However, their couplings imply only two Majorana bands also consistent with the symmetries. Since the phase carries gauge freedom, the phase difference and magnetic flux are more physically meaningful. Indeed, the flux given by Eq. (3) and $\nabla\theta$ from Eq. (5) preserve the original lattice translational symmetry, supporting the two-band structure of our Majorana crystal model.

Our theory and its application to quarter-metal superconductivity in rhombohedral graphene rely on the C_{3z} symmetry of the parent phase, which pins vortices and antivortices to distinct triangular sublattices. Strong Fermi-surface anisotropy instead favors nematic order, whose breaking of C_{3z} symmetry unpins vortices and antivortices, allowing their annihilation and stabilizing a FF state with 1D phase modulation. Recent experiments on rhombohedral hexalayer graphene report a nematic transition in the quarter-metal phase [51, 52], which may provide such an example. Starting instead from a quarter metal with an anisotropic Fermi surface but without nematic order, a recent macroscopic theory of superconductivity [35, 53, 54] ingeniously shows the possible emergence of a vortex-antivortex lattice, forming a C_{3z} -invariant pattern similar to ours. However, that pattern is incommensurate with the underlying lattice, and the emergent lattice constant is several orders of magnitude larger. Furthermore, it neglects the $e^{i2\mathbf{K} \cdot \mathbf{R}}$ factor, which we find essential.

Acknowledgement—This work was supported by the National Science Foundation under Grants No. DMR-1945351, No. DMR-2324033, and No. DMR-2414726 and by the Welch Foundation under Grant No. AT-2264-20250403.

- [1] F. Zhang, B. Sahu, H. Min, and A. H. MacDonald, *Band structure of ABC-stacked graphene trilayers*, *Phys. Rev. B* **82**, 035409 (2010).
- [2] F. Zhang, J. Jung, G. A. Fiete, Q. Niu, and A. H. MacDonald, *Spontaneous Quantum Hall States in Chirally Stacked Few-Layer Graphene Systems*, *Phys. Rev. Lett.* **106**, 156801 (2011).
- [3] R. T. Weitz, M. T. Allen, B. E. Feldman, J. Martin, and A. Yacoby, *Broken-Symmetry States in Doubly Gated Suspended Bilayer Graphene*, *Science* **330**, 812–816 (2010).
- [4] J. Martin, B. E. Feldman, R. T. Weitz, M. T. Allen, and A. Yacoby, *Local Compressibility Measurements of Correlated States in Suspended Bilayer Graphene*, *Phys. Rev. Lett.* **105**, 256806 (2010).
- [5] C. H. Lui, Z. Li, K. F. Mak, E. Cappelluti, and T. F. Heinz, *Observation of an electrically tunable band gap in trilayer graphene*, *Nat. Phys.* **7**, 944–947 (2011).
- [6] W. Bao, L. Jing, J. Velasco, Y. Lee, G. Liu, D. Tran, B. Standley,

- M. Aykol, S. B. Cronin, D. Smirnov, M. Koshino, E. McCann, M. Bockrath, and C. N. Lau, *Stacking-dependent band gap and quantum transport in trilayer graphene*, *Nat. Phys.* **7**, 948–952 (2011).
- [7] L. Zhang, Y. Zhang, J. Camacho, M. Khodas, and I. Zaliznyak, *The experimental observation of quantum Hall effect of $l=3$ chiral quasiparticles in trilayer graphene*, *Nat. Phys.* **7**, 953–957 (2011).
- [8] K. Zou, F. Zhang, C. Clapp, A. H. MacDonald, and J. Zhu, *Transport Studies of Dual-Gated ABC and ABA Trilayer Graphene: Band Gap Opening and Band Structure Tuning in Very Large Perpendicular Electric Fields*, *Nano Lett.* **13**, 369–373 (2013).
- [9] J. Velasco, L. Jing, W. Bao, Y. Lee, P. Kratz, V. Aji, M. Bockrath, C. N. Lau, C. Varma, R. Stillwell, D. Smirnov, F. Zhang, J. Jung, and A. H. MacDonald, *Transport spectroscopy of symmetry-broken insulating states in bilayer graphene*, *Nat. Nanotechnol.* **7**, 156–160 (2012).
- [10] F. Freitag, J. Trbovic, M. Weiss, and C. Schönberger, *Spontaneously Gapped Ground State in Suspended Bilayer Graphene*, *Phys. Rev. Lett.* **108**, 076602 (2012).
- [11] W. Bao, J. Velasco, F. Zhang, L. Jing, B. Standley, D. Smirnov, M. Bockrath, A. H. MacDonald, and C. N. Lau, *Evidence for a spontaneous gapped state in ultraclean bilayer graphene*, *Proc. Natl. Acad. Sci. U.S.A.* **109**, 10802–10805 (2012).
- [12] Y. Shi, S. Xu, Y. Yang, S. Slizovskiy, S. V. Morozov, S.-K. Son, S. Ozdemir, C. Mullan, J. Barrier, J. Yin, A. I. Berdyugin, B. A. Piot, T. Taniguchi, K. Watanabe, V. I. Fal’ko, K. S. Novoselov, A. K. Geim, and A. Mishchenko, *Electronic phase separation in multilayer rhombohedral graphite*, *Nature* **584**, 210–214 (2020).
- [13] T. Han, Z. Lu, G. Scuri, J. Sung, J. Wang, T. Han, K. Watanabe, T. Taniguchi, H. Park, and L. Ju, *Correlated insulator and Chern insulators in pentalayer rhombohedral-stacked graphene*, *Nat. Nanotechnol.* **19**, 181–187 (2024).
- [14] K. Liu, J. Zheng, Y. Sha, B. Lyu, F. Li, Y. Park, Y. Ren, K. Watanabe, T. Taniguchi, J. Jia, W. Luo, Z. Shi, J. Jung, and G. Chen, *Spontaneous broken-symmetry insulator and metals in tetralayer rhombohedral graphene*, *Nat. Nanotechnol.* **19**, 188–195 (2024).
- [15] T. Han, Z. Lu, Y. Yao, J. Yang, J. Seo, C. Yoon, K. Watanabe, T. Taniguchi, L. Fu, F. Zhang, and L. Ju, *Large quantum anomalous Hall effect in spin-orbit proximitized rhombohedral graphene*, *Science* **384**, 647–651 (2024).
- [16] Y. Sha, J. Zheng, K. Liu, H. Du, K. Watanabe, T. Taniguchi, J. Jia, Z. Shi, R. Zhong, and G. Chen, *Observation of a Chern insulator in crystalline ABCA-tetralayer graphene with spin-orbit coupling*, *Science* **384**, 414–419 (2024).
- [17] F. Winterer, F. R. Geisenhof, N. Fernandez, A. M. Seiler, F. Zhang, and R. T. Weitz, *Ferroelectric and spontaneous quantum Hall states in intrinsic rhombohedral trilayer graphene*, *Nat. Phys.* **20**, 422–427 (2024).
- [18] F. R. Geisenhof, F. Winterer, A. M. Seiler, J. Lenz, T. Xu, F. Zhang, and R. T. Weitz, *Quantum anomalous Hall octet driven by orbital magnetism in bilayer graphene*, *Nature* **598**, 53–58 (2021).
- [19] H. Zhou, T. Xie, A. Ghazaryan, T. Holder, J. R. Ehrets, E. M. Spanton, T. Taniguchi, K. Watanabe, E. Berg, M. Serbyn, and A. F. Young, *Half- and quarter-metals in rhombohedral trilayer graphene*, *Nature* **598**, 429–433 (2021).
- [20] S. C. de la Barrera, S. Aronson, Z. Zheng, K. Watanabe, T. Taniguchi, Q. Ma, P. Jarillo-Herrero, and R. Ashoori, *Cascade of isospin phase transitions in Bernal-stacked bilayer graphene at zero magnetic field*, *Nat. Phys.* **18**, 771–775 (2022).
- [21] A. M. Seiler, F. R. Geisenhof, F. Winterer, K. Watanabe, T. Taniguchi, T. Xu, F. Zhang, and R. T. Weitz, *Quantum cascade of correlated phases in trigonally warped bilayer graphene*, *Nature* **608**, 298–302 (2022).
- [22] H. Zhou, L. Holleis, Y. Saito, L. Cohen, W. Huynh, C. L. Patterson, F. Yang, T. Taniguchi, K. Watanabe, and A. F. Young, *Isospin magnetism and spin-polarized superconductivity in Bernal bilayer graphene*, *Science* **375**, 774–778 (2022).
- [23] J. Yang, X. Shi, S. Ye, C. Yoon, Z. Lu, V. Kakani, T. Han, J. Seo, L. Shi, K. Watanabe, T. Taniguchi, F. Zhang, and L. Ju, *Impact of Spin-Orbit Coupling on Superconductivity in Rhombohedral Graphene*, [arXiv:2408.09906](https://arxiv.org/abs/2408.09906).
- [24] H. Zhou, T. Xie, T. Taniguchi, K. Watanabe, and A. F. Young, *Superconductivity in rhombohedral trilayer graphene*, *Nature* **598**, 434–438 (2021).
- [25] Y. Zhang, R. Polski, A. Thomson, É. Lantagne-Hurtubise, C. Lewandowski, H. Zhou, K. Watanabe, T. Taniguchi, J. Alicea, and S. Nadj-Perge, *Enhanced superconductivity in spin-orbit proximitized bilayer graphene*, *Nature* **613**, 268–273 (2023).
- [26] T. Han, Z. Lu, Z. Hadjri, L. Shi, Z. Wu, W. Xu, Y. Yao, A. A. Cotten, O. Sharifi Sedeh, H. Weldeyesus, J. Yang, J. Seo, S. Ye, M. Zhou, H. Liu, G. Shi, Z. Hua, K. Watanabe, T. Taniguchi, P. Xiong, D. M. Zumbühl, L. Fu, and L. Ju, *Signatures of chiral superconductivity in rhombohedral graphene*, *Nature* **643**, 654–661 (2025).
- [27] Y.-Z. Chou, J. Zhu, and S. Das Sarma, *Intravalley spin-polarized superconductivity in rhombohedral tetralayer graphene*, *Phys. Rev. B* **111**, 174523 (2025).
- [28] M. Geier, M. Davydova, and L. Fu, *Chiral and topological superconductivity in isospin polarized multilayer graphene*, *Nat. Commun.* **17**, 232 (2025).
- [29] M. Kim, A. Timmel, L. Ju, and X.-G. Wen, *Topological chiral superconductivity beyond pairing in a Fermi liquid*, *Phys. Rev. B* **111**, 014508 (2025).
- [30] Y.-Q. Wang, Z.-Q. Gao, and H. Yang, *Chiral superconductivity from parent Chern band and its non-Abelian generalization*, [arXiv:2410.05384](https://arxiv.org/abs/2410.05384).
- [31] Q. Qin and C. Wu, *Chiral finite-momentum superconductivity in the tetralayer graphene*, [arXiv:2412.07145](https://arxiv.org/abs/2412.07145).
- [32] C. Yoon, T. Xu, Y. Barlas, and F. Zhang, *Quarter-Metal Superconductivity in Rhombohedral Graphene*, *Phys. Rev. Lett.* **136**, 026603 (2026).
- [33] G. Parra-Martínez, A. Jimeno-Pozo, V. o. T. Phong, H. Sainz-Cruz, D. Kaplan, P. Emanuel, Y. Oreg, P. A. Pantaleón, J. A. Silva-Guillén, and F. Guinea, *Band Renormalization, Quarter Metals, and Chiral Superconductivity in Rhombohedral Tetralayer Graphene*, *Phys. Rev. Lett.* **135**, 136503 (2025).
- [34] B. A. Bernevig and Y. H. Kwan, *“Berry Trashcan” Model of Interacting Electrons in Rhombohedral Graphene*, [arXiv:2503.09692](https://arxiv.org/abs/2503.09692).
- [35] F. Gaggioli, D. Guerci, and L. Fu, *Spontaneous Vortex-Antivortex Lattice and Majorana Fermions in Rhombohedral Graphene*, *Phys. Rev. Lett.* **135**, 116001 (2025).
- [36] D. F. Agterberg, J. S. Davis, S. D. Edkins, E. Fradkin, D. J. Van Harlingen, S. A. Kivelson, P. A. Lee, L. Radzihovsky, J. M. Tranquada, and Y. Wang, *The Physics of Pair-Density Waves: Cuprate Superconductors and Beyond*, *Annu. Rev. Condens. Matter Phys.* **11**, 231–270 (2020).
- [37] R. Casalbuoni and G. Nardulli, *Inhomogeneous superconductivity in condensed matter and QCD*, *Rev. Mod. Phys.* **76**, 263–320 (2004).
- [38] J. J. Kinnunen, J. E. Baarsma, J.-P. Martikainen, and P. Törmä, *The Fulde–Ferrell–Larkin–Ovchinnikov state for ultracold fermions in lattice and harmonic potentials: a review*, *Rep.*

- Prog. Phys. **81**, 046401 (2018).
- [39] E. Fradkin, S. A. Kivelson, and J. M. Tranquada, *Colloquium: Theory of intertwined orders in high temperature superconductors*, *Rev. Mod. Phys.* **87**, 457–482 (2015).
- [40] T. Kloss, X. Montiel, V. S. de Carvalho, H. Freire, and C. Pépin, *Charge orders, magnetism and pairings in the cuprate superconductors*, *Rep. Prog. Phys.* **79**, 084507 (2016).
- [41] P. Fulde and R. A. Ferrell, *Superconductivity in a Strong Spin-Exchange Field*, *Phys. Rev.* **135**, A550–A563 (1964).
- [42] A. I. Larkin and Y. N. Ovchinnikov, *Nonuniform state of superconductors*, *Sov. Phys. JETP* **20**, 762–770 (1965).
- [43] A. Melikyan and Z. Tešanović, *Dirac-Bogoliubov-deGennes quasiparticles in a vortex lattice*, *Phys. Rev. B* **76**, 094509 (2007).
- [44] J. M. Murray and O. Vafek, *Majorana bands, Berry curvature, and thermal Hall conductivity in the vortex state of a chiral p-wave superconductor*, *Phys. Rev. B* **92**, 134520 (2015).
- [45] V. Cvetkovic and O. Vafek, *Berry phases and the intrinsic thermal Hall effect in high-temperature cuprate superconductors*, *Nat. Commun.* **6**, 6518 (2015).
- [46] The delta function, i.e., zero core size, is consistent with the low-density and flat-band nature of graphene superconductivity.
- [47] M. P. Marder, *Condensed Matter Physics*, 2nd ed. (Wiley, 2015).
- [48] We have used $\nabla\theta - (2e/\hbar c)A = 0$, which is valid when the penetration depth $\lambda_L = 0$ or when the supercurrent $j_s = 0$ (in equilibrium without superflow or outside a vortex core). The $\lambda_L > 0$ case will be addressed in *Discussion*.
- [49] R. R. Biswas, *Majorana Fermions in Vortex Lattices*, *Phys. Rev. Lett.* **111**, 136401 (2013).
- [50] F. D. M. Haldane, *Model for a Quantum Hall Effect without Landau Levels: Condensed-Matter Realization of the "Parity Anomaly"*, *Phys. Rev. Lett.* **61**, 2015–2018 (1988).
- [51] R. Q. Nguyen, H.-T. Wu, E. Morissette, N. J. Zhang, P. Qin, K. Watanabe, T. Taniguchi, A. W. Hui, D. E. Feldman, and J. I. A. Li, *A Hierarchy of Superconductivity and Topological Charge Density Wave States in Rhombohedral Graphene*, [arXiv:2507.22026](https://arxiv.org/abs/2507.22026).
- [52] P. Qin, H.-T. Wu, R. Q. Nguyen, E. Morissette, N. J. Zhang, K. Watanabe, T. Taniguchi, and J. I. A. Li, *Extreme Anisotropy in the Metallic and Superconducting Phases of Rhombohedral Hexalayer Graphene*, [arXiv:2504.05129](https://arxiv.org/abs/2504.05129).
- [53] M. Christos, P. M. Bonetti, and M. S. Scheurer, *Finite-momentum pairing and superlattice superconductivity in valley-imbalance rhombohedral graphene*, [arXiv:2503.15471](https://arxiv.org/abs/2503.15471).
- [54] A. Gil and E. Berg, *Charge and pair density waves in a spin and valley-polarized system at a Van-Hove singularity*, [arXiv:2504.19321](https://arxiv.org/abs/2504.19321).